

## RESEARCH ARTICLE

# Internodular functional connectivity in heterotopia-related epilepsy

Hui Ming Khoo<sup>1,2</sup> , Nicolás von Ellenrieder<sup>1</sup>, Natalja Zazubovits<sup>1</sup>, Jeffery A. Hall<sup>1</sup>, François Dubeau<sup>1</sup> & Jean Gotman<sup>1</sup>

<sup>1</sup>Montreal Neurological Institute and Hospital, McGill University, Montreal, Quebec, Canada

<sup>2</sup>Department of Neurosurgery, Osaka University Graduate School of Medicine, Suita, Japan

## Correspondence

Hui Ming Khoo, Montreal Neurological Institute and Hospital, McGill University, 3801 University Street, Montreal, Quebec, Canada H3A 2B4. Tel: +1-514-398-1952; Fax: +1-514-398-8106; E-mail: hui.ming.khoo@mail.mcgill.ca

## Funding Information

This work was supported by the Canadian Institutes of Health Research (FDN 143208). H.M.K. is supported by Grant-in-Aid for Scientific Research (18H06261) from the Ministry of Education, Culture, Sports, Science and Technology of Japan, and was supported by Mark Rayport and Shirley Ferguson Rayport fellowship in epilepsy surgery and the Preston Robb fellowship of the Montreal Neurological Institute (Canada), a research fellowship of the Uehara Memorial Foundation (Japan), travel grants from Osaka Medical Research Foundation for Intractable Diseases (Japan) and Japan Epilepsy Research Foundation (Japan). F.D. is supported by a grant from Savoy Foundation (Canada).

Received: 28 February 2019; Accepted: 5 March 2019

*Annals of Clinical and Translational Neurology* 2019; 6(6): 1010–1023

doi: 10.1002/acn3.769

## Introduction

Nodular heterotopia is a developmental brain malformation well-known to be associated with epilepsy.<sup>1,2</sup> However, the role of the heterotopic nodule itself in epileptogenicity is still a matter of debate. Electrophysiological studies showed that heterotopic nodules can be intrinsically epileptogenic, but other studies indicate that a large epileptic network, rather than solely a nodule, is indeed responsible for epileptogenicity.<sup>3–6</sup> This

## Abstract

**Objective:** A vast network involving the nodules and overlying cortices is believed to be responsible for the epileptogenicity in gray matter heterotopia with multiple nodules, which often associated with difficult-to-treat epilepsy. We sought to determine if functional magnetic resonance imaging (fMRI) could detect internodular functional connectivity (FC), and if this connectivity reflects an actual synchronized neuronal activity and partakes in epileptogenicity. **Methods:** We studied 16 epilepsy patients with multiple heterotopic nodules; eight underwent subsequent intracerebral EEG. We examined the internodular FC using fMRI and its correspondence with internodular synchrony of intracerebral interictal activity. We then compared the spreading speed of ictal activity between connected and unconnected nodules; and the FC among possible combinations of nodule pairs in terms of their involvement at seizure onset. **Results:** Seventy nodules were studied: 83% have significant connection to at least one other nodule. Among the 49 pairs studied with intracerebral EEG, (1) synchronized interictal activity is more prevalent in fMRI-connected pairs ( $P < 0.05$ ), (2) ictal activity spreads faster between connected pairs ( $P < 0.0001$ ), and (3) stronger FC was observed between pairs in which both nodules were involved at seizure onset ( $P < 0.01$ ). **Interpretation:** fMRI could reliably and noninvasively detect the FC between heterotopic nodules. These functional connections correspond to the synchrony of interictal epileptic activity between the nodules and to the ability of nodules to generate synchronous seizure onsets or rapid seizure spread. These findings may help in understanding the complexity of the epileptogenic network in multiple heterotopic nodules and better targeting the likely epileptogenic nodules.

network could involve the heterotopic nodules and the cortices.<sup>7–9</sup>

Literally, “heterotopia” refers to normal looking neurons located in an abnormal position. The periventricular nodular heterotopia (PNH) can be unilateral or bilateral, isolated or multiple and located anywhere along the lateral ventricles. Neurons within the heterotopia are known to have abnormal synaptic organization,<sup>6,10,11</sup> and studies using different techniques, including histology, intracerebral EEG (iEEG), functional magnetic resonance imaging

(fMRI), and diffusion tensor imaging, showed connectivity between the nodules and cortical areas<sup>2,7,10–15</sup>; and among the nodules themselves in some patients.<sup>10–12</sup>

Epilepsy related to PNH is usually difficult to treat; it is often drug-resistant and surgical resection of the temporal lobe, as originally performed because of the frequent temporal lobe symptomatology and EEG findings, is unlikely to be effective.<sup>2,16</sup> Better surgical outcomes have been reported in small cohort studies in which the patients were studied extensively with iEEG including the heterotopic nodules.<sup>4,6</sup> Recently, ablation techniques (radiofrequency thermo-coagulation, or laser ablation) are becoming popular because of the ability to address multiple targets less invasively. However, even with ablations, a better seizure outcome is still more likely in patients with a single nodule compared to those with multiple nodules.<sup>17,18</sup> In patients with multiple nodules, good seizure outcome is also achievable when the ablation targets extensively the epileptic network that includes all or several of the heterotopic nodules.<sup>17</sup> Based on these observations, the role of each nodule in the epileptic network of patients with multiple nodules may be heterogeneous and unique to each patient. We hypothesize that functional connectivity (FC) between nodules is one of the factors that determines the role of the nodules within the epileptic network. Connectivity has been studied in these patients, particularly connections between nodules and cortices.<sup>7,12,15</sup> However, none of the studies have specifically addressed the FC between the nodules themselves.

We want to know if an actual neuronal-based FC exists between nodules and, if it does, what is the role of this FC in epileptogenesis. We first examine noninvasively the FC between nodules using fMRI. Then, we sought to understand the electrophysiological basis of this fMRI-measured connectivity, in particular whether the neuronal activity is synchronized and corresponds to an epileptic network in which the nodules interact. To study this relationship, we analyzed the intracerebral interictal and ictal epileptic activity recorded using electrodes inserted in at least two distinct heterotopic nodules. Our findings provide new insights into neuronal correlates of hemodynamic-based FC between distant heterotopia, and offer a novel noninvasive approach to identify key nodules within the epileptic network. This should contribute to a better planning of treatment for these difficult-to-treat patients with epilepsy.

## Methods

### Study population

From the database of patients who underwent fMRI as part of the combined EEG-fMRI study between April

2006 and September 2018, we identified 28 consecutive patients with PNH-related epilepsy. Twelve patients had a single nodule or a cluster of multiple but inseparable contiguous nodules and thus were excluded. Sixteen patients were included (Table 1); PNH were unilateral in five and bilateral in 11. The nodules were located along the temporal horns, trigones or occipital horns in 13 patients (patients 2, 4–13, 15, and 16); along the frontal horns, anteriorly, and the temporal horns and trigones, posteriorly in two others (patients 1 and 3); and along the body of the right lateral ventricle and ipsilateral trigone in one (patient 14). Four patients had additional cortical gyration anomalies (patients 1–3 and 8). Eight of these 16 patients (patients 1–8) with multiple heterotopia and focal drug-resistant epilepsy subsequently underwent an iEEG study as part of their presurgical evaluation, allowing comparison between fMRI and iEEG findings.

Each patient gave written informed consent for the EEG-fMRI study approved by the Research Ethics Committee of Montreal Neurological Institute and Hospital.

### Image acquisition

We used the MRI data collected during the EEG-fMRI study of these patients, acquired on a 3-Tesla MRI scanner (Siemens, Trio, Germany), identical to previous studies.<sup>19,20</sup> The scalp EEG data acquired simultaneously were used for vigilance state scoring (see below) but not used in FC analysis. The fMRI data were collected in continuous 6-min scans for a total of seven to 15 scans with patients at rest, using the T2\*-weighted echo planar imaging sequences: Until July 2008: repetition time = 1.75 sec; echo time = 30 msec; 64 × 64 matrix; 25 slices; voxel, 5 × 5 × 5 mm; flip angle 90 degrees; and from July 2008 to April 2017: repetition time = 1.9 sec; echo time = 25 msec; 64 × 64 matrix; 33 slices; voxel, 3.7 × 3.7 × 3.7 mm; flip angle 90 degrees; from May 2017: repetition time = 1.9 sec; echo time = 25 msec; 64 × 64 matrix; 34 slices; voxel, 3.7 × 3.7 × 3.7 mm; flip angle 70 degrees. A T1-weighted anatomic (magnetization-prepared rapid acquisition gradient echo) image was acquired using the following sequences: Until July 2008: 1-mm slice thickness; 256 × 256 matrix; repetition time = 23 msec; echo time = 7.4 msec; flip angle 30 degrees and from July 2008 to April 2017: 1-mm slice thickness; 256 × 256 matrix; repetition time = 23 msec; echo time = 4.18 msec; flip angle 90 degrees; from May 2017: 1-mm slice thickness; 256 × 256 matrix; repetition time = 23 msec; echo time = 4.18 msec; flip angle 9 degrees. The T1-weighted image was used for co-registration with functional images and identification of heterotopic nodules.

**Table 1.** Clinical and electrophysiological characteristics (N = 16).

Pt ID	Age (yr)	Sex	Age at onset (yr)	Seizure semiology	Topology of heterotopic nodules	Total no. of nodules	Location/number of nodules implanted with stereo-EEG	Scalp EEG findings
1	39	F	12	Chest-epigastric sensation, activity arrest, staring, head-nodding, oral and manual automatisms.	Bilat frontal horns (L:1, R:1); bilat trigones (L:2, R:1)	5	L trigone/1 R trigone/1	Interictal: Independent IED over R and L F, T and P region. Ictal: independent onset over R and L T region.
2	21	F	11	Speech arrest, staring, oral automatisms, bimanual automatisms, head and eye deviation to R, L arm dystonia. Occ FBTCs.	Bilat trigones (L:3, R:2)	5	L trigone/1 R trigone/1	Interictal: IED over R T-P region, sometimes extending to the whole R hem or bilaterally. Ictal: onset over R PQ or diffuse with predominance over R TP regions.
3	35	M	20	Verbal vocalization and hand rubbing.	Bilat frontal horns (L:1, R:5); bilat, extending from trigones to temporal horns (L:1, R:1)	8	L trigone-temporal horn/1 L frontal horn/1 R trigone-temporal horn/1 R frontal horn/1	Interictal: Independent IED over L F-T, L T or bilateral PQ regions. Ictal: onset max over L T region.
4	19	M	12	Unresponsive, activity arrest, eyes and head deviation to L	Unilat R temporal horn (R:1); bilat occipital horns (L:1, R:1)	3	L occipital horn/1 R temporal horn/1 R occipital horn/1	Interictal: independent IED over R and L F-T regions. Ictal: generalized background attenuation, then max over R F region.
5	25	F	16	Looked confused, manual automatisms, chewing, staring.	Bilat trigones (L:2, R:2)	4	L trigone/2 R trigone/2	Interictal: IED over L F-T region. Ictal: onset over L T region.
6	25	M	14	Déjà vu. Manual automatisms.	Bilat temporal horns (L:1, R:1); bilat trigones (L:3, R:4)	9	L temporal horn/1 L trigone/3 R temporal horn/1 R trigone/2	Interictal: independent IED over R and L F-T regions Ictal: not recorded.
7	43	F	16	Unresponsive, staring, manual automatisms, chewing. Occ FBTCs.	Bilat trigones (L:2, R:2)	4	L trigone/2 R trigone/1	Interictal: independent IED over R and L PQ and L F-T region. Ictal: independent onset over L T region and R hemisphere.
8	26	F	14	Numb sensation of L hand & fingers, staring, R hand repetitive movements, R arm dystonic posture. Occ FBTCs.	Unilat L trigone (1) and occipital horn (1)	2	L trigone/1 L occipital horn/1	Interictal: Independent IED over L F-T, F-C-T regions and PQ. Ictal: onset over L posterior T region.
9	18	M	15	Activity arrest, repetitive speech, bimanual automatisms.	Bilat trigones (L:2, R:1)	3	Not applicable	Interictal: independent IED over L PQ, R and L F-T regions. Ictal: onset over L PQ.
10	33	F	15		Unilat L trigone (1) and occipital horn (5)	6	Not applicable	Interictal: IED over L PQ. Ictal: onset over L T-P region

(Continued)

Table 1. Continued.

Pt ID	Age (yr)	Sex	Age at onset (yr)	Seizure semiology	Topology of heterotopic nodules	Total no. of nodules	Location/number of nodules implanted with stereo-EEG	Scalp EEG findings
11	22	F	17	Feeling of throat tightness, flushing, tunnel vision, speech arrest, loss of awareness.	Unilat L trigone (2)	2	Not applicable	Interictal: IED over L F-T region. Ictal: not recorded.
12	52	M	17	Nausea, loss of awareness, head deviation to R, R face and arm jerk. Visual distortion, head deviation to L, lip smacking and swallowing, unresponsiveness, staring, auditory distortion.	Bilat trigones (L:2, R:2)	4	Not applicable	Interictal: independent IED over L F-T region and R PQ. Ictal: onset over R F-T region.
13	19	M	16	Chilly sensation in the lumbar region, activity arrest, loss of awareness, arm-crossing.	Bil trigones (L:1, R:2)	3	Not applicable	Interictal: IED over R F-T and T regions. Ictal: not recorded.
14	19	F	2	Sensation of chest pressure, facial grimace, fearful look in the face, moaning, head deviation to the R, staring.	Unilat body of R lateral ventricle (1); unilat R trigone (1)	2	Not applicable	Interictal: IED over R C and sometimes R hemisphere. Ictal: not localizing (muscle artifacts)
15	19	F	0	Activity arrest, head flexion, raise of both arms, loss of awareness, head version to the L, L hemibody clonus. Occ FBTCs.	Unilat R temporal horn (1); unilat R trigone (2)	3	Not applicable	Interictal: Independent IED over R F-T and C regions. Sometimes generalized IED. Ictal: onset over R T region.
16	28	M	24	Anxiety and/or rising sensation from chest to head, blurry vision, staring, manual and oral automatisms, agitation.	Bilat, extending from trigones to temporal horns (L:4, R:3)	7	Not applicable	Interictal: IED over R F-T region. Ictal: onset over R PQ.

Bilat, bilateral; C, central; F (in the column of sex); female; F, frontal; FBTCs, focal to bilateral tonic-clonic seizures; L, left; M, male; occ, occasional; P, parietal; PQ, posterior quadrant; R, right; T, temporal; unilat: unilateral.

## Identification and outline of heterotopic nodules as the regions of interest

On the T1-weighted anatomic image in the native space of each patient, we visually identified and manually outlined each discrete heterotopic nodule (either an individual nodule or an inseparable contiguous cluster of nodules) slice by slice in the axial plane, as a region of interest (ROI), using MRIcron software (<http://people.cas.sc.edu/rorden/mricron/index.html>).

## Functional connectivity between heterotopic nodules in fMRI

The T1-weighted anatomic image of each patient was automatically segmented into gray matter, white matter and cerebrospinal fluid using FreeSurfer (<http://freesurfer.net/>). To ensure that the heterotopic nodules were totally excluded from the white matter segment, we used the ROIs outlined above to reclassify any mis-segmented heterotopic nodule to the gray matter segment, using an in-house custom script created in MATLAB (MathWorks, Natick, USA). This is to make sure that the blood oxygenation level-dependent signal in the nodules was not regressed out because the white matter and cerebrospinal fluid segments were entered as nuisance regressors in subsequent FC analysis (see below).

FC analyses were performed in the patients' native space using a validated FC toolbox (CONN version 17.f) (<http://www.nitrc.org/projects/conn>)<sup>21</sup> operated on Statistical Parametric Mapping-8 (SPM8) ([www.fil.ion.ucl.ac.uk/spm](http://www.fil.ion.ucl.ac.uk/spm)) and MATLAB. The functional images were preprocessed as follows: for each patient, the echo planar images were realigned to the first volume of the first scan, unwarped and slice-time corrected, scrubbed for outlier scans (using ART-based functional outlier detection) and then registered to the T1-weighted anatomic image, without normalization. ART-based functional outlier detection and scrubbing was used in the preprocessing pipeline in CONN to account for movement of individual patients. Spatial smoothing was not performed to avoid contamination of blood oxygenation level-dependent signal in the PNH by adjacent cerebrospinal fluid in the ventricles.<sup>22</sup>

We assessed FC between nodules using ROI-to-ROI correlations. Echo planar images were segmented using the nodule ROIs and the time series representing each nodule were extracted by averaging the time series of all voxels within that nodule. A band-pass filter ( $0.008 \text{ Hz} < f < 0.09 \text{ Hz}$ ) was applied to remove high frequency noise and linear drift artifacts. Head motion (realignment parameters), white matter, and cerebrospinal fluid segments were entered as nuisance regressors in

first-level analyses. Before computing connectivity measures, each of these effects was regressed out of the blood oxygenation level-dependent signal using the component-based noise correction (ACompCor) strategy, which increases sensitivity and selectivity and allows for a high degree of interscan reliability.<sup>21</sup>

ROI-to-ROI connectivity measures were based on correlation analyses. Pearson's correlation coefficients of the representative time series were calculated for each possible nodule pair in each scan for each patient (each patient had seven to 15 6-min scans). The *r*-values were then normalized using the Fisher's transformation to derive the connectivity measures. Scan-specific connectivity matrices were produced in a first-level analysis. Second-level ROI-to-ROI analyses were then conducted to identify the correlated ROIs common across scans of each patient using a one-sample *t*-test on the connectivity matrices derived from the first level analysis of each patient. Significantly connected pairs of ROIs were identified using a corrected  $P < 0.05$  (patient-specific Bonferroni correction, two-sided), labeled "connected" and otherwise "unconnected". The average connectivity measure was calculated, back-transformed to *r*-value and used wherever applicable.

## Intracerebral EEG acquisition

Multi-contact stereo-EEG electrodes (electrodes manufactured on-site, contact spacing 5 mm, nine contacts, 0.5–1 mm length each, or commercially available electrodes (DIXI Medical, Besancon, France), contact spacing 3.5 mm, 15–18 contacts, 2 mm length each) were implanted using image-guided stereotaxy with or without robotized surgical assistant.<sup>23,24</sup> The deepest contacts were aimed at the mesial structures and the most superficial placed in the lateral cortical mantle. Clinical diagnostic data (seizure semiology, scalp EEG, structural MRI, and FDG-PET and ictal SPECT when available) were considered to determine the planning of electrode placement. iEEGs were recorded using the Harmonie EEG system (Stellate, Montreal, Canada) prior to September 2016 and the Neurofax EEG-1200A system (Nihon-Kohden, Tokyo, Japan) thereafter. iEEG recordings were acquired at a sampling rate of 2000 Hz in all patients and band-pass filtered at 0.3–500 Hz (Harmonie) or at 0.016–600 Hz (Neurofax) except for patient 7 (acquired at 200 Hz and band-pass filtered at 0.3–70 Hz), with a referential electrode placed over the parietal lobe contralateral to the suspected epileptogenic zone. All iEEG data were analyzed using a bipolar montage between two adjacent contacts on each electrode. Electrooculography-electromyography (EOG-EMG) and subdermal thin wire electrodes,<sup>25</sup> placed at F3, F4, Fz,

C3, C4, Cz, P3, P4, and Pz were used, allowing identification of sleep stages.

### Selection of interictal iEEG recording

We selected the first suitable interictal recordings at least 72 h postimplantation to avoid the potential influence of anesthesia on sleep and the acute effect of electrode placement.<sup>26</sup> To avoid the potential influence of seizures, we excluded recordings where a secondarily generalized seizure was present during the 12 h, or a clinical EEG seizure during the 6 h, or asymptomatic EEG seizure during the 2 h prior to the evaluation period and any EEG seizure during the 2 h following the evaluation period. Periods contaminated with artifacts were excluded.

### Matching of interictal iEEG data with fMRI data

Because the iEEG and the fMRI were not measured simultaneously, we selected the best-matched iEEG data of each patient to enable a fair comparison with the fMRI findings using the following procedure:

#### Matching the vigilance state

We used the EEG acquired simultaneously with the fMRI to assess the vigilance state during each scan, identically to our previous study.<sup>20</sup> In brief, sleep or wakefulness during fMRI study were scored manually using EEG features described in the AASM criteria.<sup>27</sup> Wakefulness was defined as presence of alpha rhythm in greater than 50% of the recording or the absence of sleep-related EEG component. The presence of sleep-related EEG component indicated sleep. We scored the vigilance state (sleep or wakefulness) for each fMRI scan to enable selection of iEEG data that match approximately the vigilance state of each fMRI scan for each patient. For the iEEG recordings, we used simultaneous video recording, subdermal scalp EEG, EOG-EMG during the iEEG study or combinations of these approaches to identify vigilance states.

#### Matching the duration of iEEG recording and fMRI total acquisition time

We sampled the iEEG recording in multiple 6-min consecutive segments and included the same number of segments as the number of fMRI scans acquired for each patient. For patient 7, continuous iEEG data were not available due to the archiving process; we sampled multiple segments (1 to 2-min each) and concatenated them to obtain multiple 6-min segments.

### Co-registration of heterotopic nodule ROIs and iEEG electrode contacts

Post-implantation MRI or CT, routinely obtained for electrode localization, and the T1-weighted anatomic image used for the outline of heterotopia ROIs were co-registered linearly using MINC tools (<https://github.com/BIC-MNI>). The trajectory of each electrode was manually indicated in the post-implantation MRI or CT. The coordinates of each electrode contact were computed from the distance between contacts and the coordinates of the entry and target of the electrodes, using our visualization platform for neuro-navigation (IBIS).<sup>28</sup>

We visually identified iEEG electrode contacts located within the nodules with the assistance of the nodule ROIs (see above). iEEG channels (two adjacent contacts made one channel) located within the nodules (*nodule channels*) were selected using the following criteria: (i) both electrode contacts were located within the nodule ( $N = 44$ ); and (ii) one contact located within the nodule and one in the adjacent white matter ( $N = 35$ ), representing signal predominantly from the nodule because the signal in the white matter is low in amplitude.<sup>29</sup> To lower the chance of including signal from gray matter other than the heterotopias, we did not include channels in which one of the electrode contacts was located in adjacent gray matter even if the other contact was located within a nodule.

### Analysis of iEEG functional connectivity between nodule channel pairs

To quantify the iEEG FC between nodule channels pairs, we used identical methods as in a previous study.<sup>20</sup> In brief, we first computed a surrogate signal that reflects the presence of interictal epileptic discharges (IEDs) in each channel, and then computed the correlation coefficient between pairs of these surrogate signals. If IEDs occurred in two channels at roughly the same time, the correlation coefficient is high, and if IEDs did not occur synchronously, or if there were no IEDs, the correlation coefficient is low. We used the gamma band envelope of the raw iEEG as the surrogate signal, which we obtained by high-pass filtering the raw iEEG (forward and backward application of an elliptic IIR filter of order three, 30 Hz cut-off, 60 dB attenuation, 0.5 dB ripple in pass band), and computing the root mean square value of the filtered signal in a moving window of 200 msec. We choose to use the gamma band envelope because it most likely represents the presence of IEDs.<sup>20</sup>

To allow fair comparison between iEEG-based and fMRI-based FC, we used for iEEG identical analysis and statistics to identify connected nodules as was used for fMRI. Pearson's correlation coefficients of the iEEG were

calculated in all possible nodule channel pairs in each 6-min segment for each patient. Segment-specific connectivity matrices were produced in a first-level analysis. To perform the second-level analysis, the  $r$ -values were then normalized using Fisher's transformation to derive the connectivity measure. The second-level analyses were conducted to identify the pairs correlated consistently across segments of each patient using a one-sample  $t$ -test on the connectivity matrices derived from the first level analysis of each patient. Significantly connected pairs were identified using a corrected  $P < 0.05$  (patient-specific Bonferroni correction). A pair of heterotopic nodules can have multiple channel pairs between the two nodules if multiple electrodes were implanted within one nodule. A pair of nodules was considered connected if at least one of the channel pairs was significantly connected. These nodules were labeled "connected" and otherwise "unconnected".

### Functional connectivity and involvement of nodules at seizure onset

In order to analyze the correspondence between FC and involvement of nodules at seizure onset, we determined the channels involved at seizure onset; two electroencephalographers (FD and HMK) reviewed the recordings. Channels showing the first unequivocal EEG change from the background activity that led to a seizure discharge and those within 500 msec from the seizure onset were considered involved at seizure onset. A nodule was considered involved at seizure onset if at least one of its nodule channels was involved at seizure onset. We separated the nodule pairs into three groups in terms of involvement at seizure onset ("both nodules involved", "only one nodule involved", and "neither nodule involved"); and compared the FC among these three groups.

### Evaluation of spread of ictal activity between two nodule channels

To evaluate the difference in ictal activity spread between connected and unconnected nodules, we measured the latency between the appearances of ictal activity in channels located in two nodules. Each nodule channel was inspected and an unequivocal EEG change from its background activity that led to a seizure discharge was marked as the appearance of ictal activity on that channel. This ictal activity could be an activity of seizure onset or of seizure spread but it corresponds to the earliest appearance of ictal activity in that channel. The marking was independent of the location of the seizure onset zone. We computed the latency of appearance of ictal activity between two nodule channels for all possible combinations of channel pairs between two heterotopic nodules during each seizure. This was performed for all seizures.

To control for the effect of distance between channels on latency, we also computed the speed of ictal activity spread between channels. The midpoint between two adjacent iEEG electrode contacts was considered the physical location of a bipolar channel and the distances between channels were computed based on the coordinates of the electrode contacts. We separated these channel pairs into two groups in terms of FC between nodules as defined above ("connected" and "unconnected", according to fMRI); and compared latency and speed between these two groups.

### Statistical analysis

We measured the FC between heterotopic nodules in both fMRI and iEEG using Pearson's correlation coefficient. The Bonferroni correction was applied as appropriate to each set of analysis to adjust for multiple comparisons, maintaining the level of significance at 0.05. We assessed the correspondence of connectivity measures between fMRI and iEEG, and between nodules located within ipsi- and contralateral hemispheres using Fisher's exact test, with the null hypothesis being no correspondence. Wilcoxon rank sums test was applied for comparisons of medians between two groups. Steel-Dwass test was applied for comparisons of medians between three or more groups. Level of significance was set at  $P < 0.05$  for each test.

### Data availability

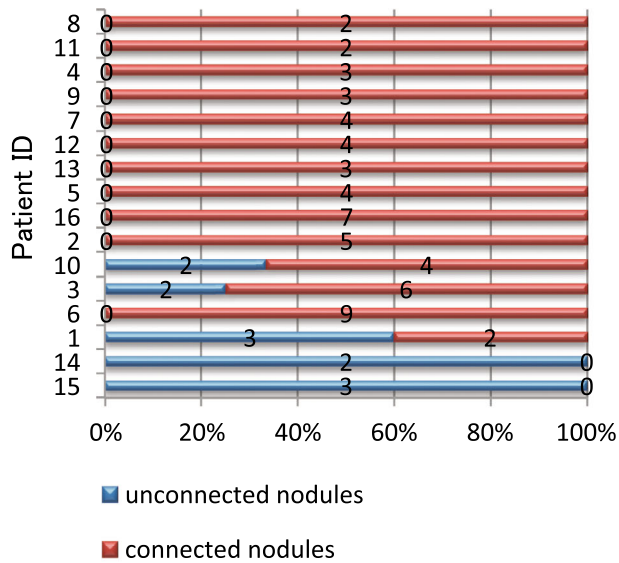
Anonymized data not published within this article will be made available upon request from any qualified investigator, subject to approval by the research ethics board of the Montreal Neurological Institute and Hospital.

## Results

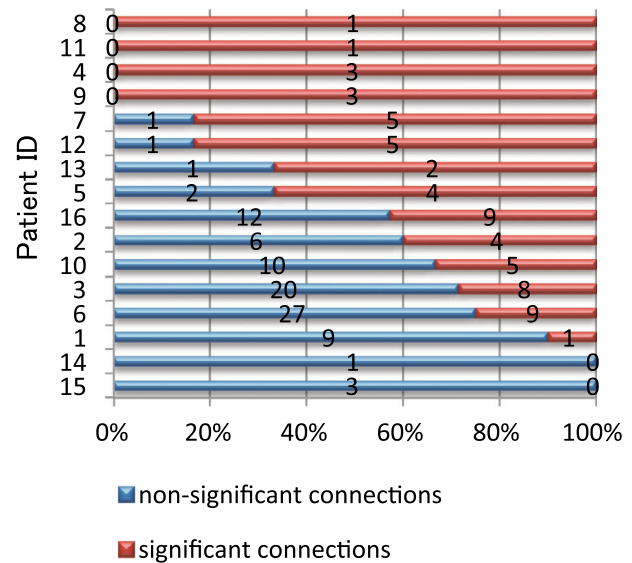
### fMRI and iEEG functional connectivity between heterotopic nodules

The patients had two to nine separable noncontiguous heterotopic nodules, with different distributions (Table 1). In the fMRI analysis, 58 of 70 nodules (83%) were connected to at least one other nodule. All the nodules in a patient were connected to at least one other nodule in 11 of the 16 patients, some of the nodules were connected in three, and none of the nodules were connected in two (Fig. 1A). Significant connections accounted for more than half of the possible combinations of nodule pairs per patient in eight patients (Fig. 1B). Connections exist between nodules regardless of the hemisphere in which the two nodules were located: there was no difference in the likelihood of two nodules being connected when comparing nodule pairs located

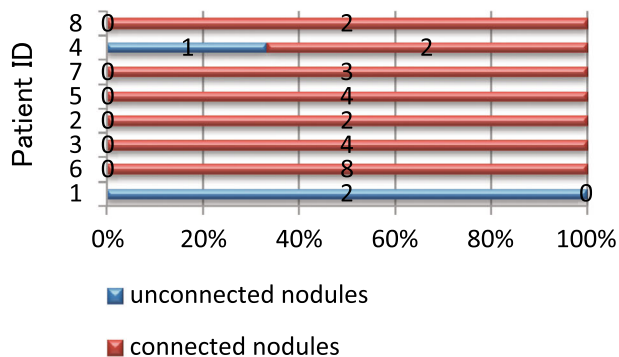
(A) fMRI – nodules



(B) fMRI – connections



(C) iEEG – nodules



(D) iEEG - connections

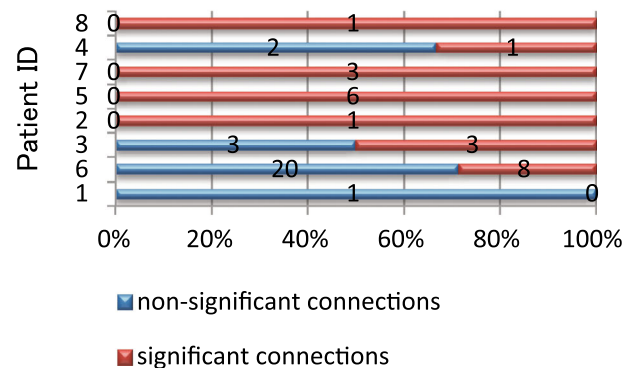


**Figure 1.** Functional connectivity between heterotopic nodules. The numbers on the Y-axis are patient IDs corresponding to that indicated in Table 1. (A) Proportion of connected and unconnected nodules in each patient based on functional MRI (fMRI) analysis and (C) based on intracerebral EEG (iEEG) analysis. Functional connectivity analysis based on iEEG was available only in the eight patients who subsequently underwent iEEG study. For instance, patient 8 has two nodules and they are connected on fMRI; both were implanted and they are also connected on iEEG; patient 1 has five nodules; two are connected on fMRI and three are not; only two of these nodules were implanted and they are not connected on iEEG. (B) Proportion of significant and nonsignificant connections of the possible combinations of nodule pairs in each patient based on fMRI analysis and (D) based on iEEG analysis. For instance, in Patient 7, there are six possible connections since the patient has four nodules (see part A); five of the six are significant on fMRI and one is not; Patient 7 has three implanted nodules (see part C), resulting in three possible connections, which are all significant on iEEG.

within the same hemisphere to those located in different hemispheres ( $P = 1.000$ ).

All eight patients who underwent iEEG (patients 1–8, Table 1) had at least two nodules implanted with at least one electrode. Analysis of the iEEG revealed similar findings as in fMRI: all nodules are connected to at least one other nodule in all except two patients (Fig. 1C). Among the implanted nodules, significant connections accounted

for more than half of the combinations of nodule pairs per patient in four of the eight patients (Fig. 1D).

### Correspondence between functional connectivity measured by fMRI and iEEG

Connectivity between heterotopic nodules measured by fMRI generally corresponded to the connectivity

**Table 2.** Correspondence between connectivity measured using functional MRI and connectivity measured using intracerebral EEG.

		Functional MRI	
		Unconnected	Connected
a. All nodule pairs			
Intracerebral EEG	Unconnected	18	8
	Connected	7	16
b. Each nodule in the pairs located in different hemisphere			
Intracerebral EEG	Unconnected	11	5
	Connected	3	11

$P = 0.0101$  (Fisher's exact test).

$P = 0.0136$  (Fisher's exact test).

measured by iEEG. Among heterotopic nodule pairs of each patient studied with iEEG ( $N = 49$  pairs), the likelihood of two nodules being connected on iEEG was significantly higher between fMRI-connected than between fMRI-unconnected nodules, when analyzing the gamma envelope of the iEEG ( $P < 0.05$ , Table 2a). See Figure 2 for an example. This correspondence holds up even in nodules from different hemispheres ( $P < 0.05$ , Table 2b).

### Difference in seizure spread between connected and unconnected nodules

The 1302 channel pairs between nodules were analyzed: 711 pairs were between fMRI-unconnected and 591 pairs were between fMRI-connected nodules. The latency between the appearances of ictal activity in two channels of a pair was significantly shorter for connected nodule pairs compared with that of unconnected nodule pairs ( $P < 0.0001$ ) (Fig. 3A). Similarly, the speed of ictal activity spread was significantly higher between connected nodule pairs compared with unconnected nodule pairs ( $P < 0.0001$ ) (Fig. 3B). The significance of the result on speed indicates that it is not only because connected nodules are physically closer that the latency is shorter. The speed of ictal activity spread was not significantly different between connected nodule pairs located within the same and those located in different hemispheres (22 mm/sec vs. 71 mm/sec,  $P = 0.8549$ ).

### Effect of functional connectivity between heterotopic nodules on epileptogenicity

To explore the effect of FC on epileptogenicity, we compared the FC (represented with Pearson's  $r$ -value) among three possible combinations of the heterotopic nodule pairs in terms of their involvement at seizure onset: both nodules involved, only one nodule involved, and neither

nodule involved. The  $r$ -value was significantly higher in the combination in which both nodules were involved at seizure onset compared with the other two combinations ( $P = 0.0059$  for "both nodules involved vs. only one nodule involved";  $P = 0.0053$  for "both nodules involved vs neither nodule involved") (Fig. 4).

## Discussion

### Functional connectivity between heterotopic nodules is prevalent

This study demonstrated that FC between heterotopic nodules is more prevalent than what has been found in the few studies addressing this issue,<sup>10–12</sup> and that these functional connections can be detected using noninvasive functional MRI. Heterotopic nodules consist of neuron clusters that failed radial migration from the embryonic ventricular zone to the developing cerebral cortex.<sup>30,31</sup> The mechanism of how multiple heterotopic nodules are formed and how these discrete nodules are related to each other is unknown. Structural connection among nodules appears to be less common than functional connections<sup>10,12</sup>: Hannan et al. reported structural connectivity between adjacent nodules in only one of the four patients studied; and Christodoulou et al. reported structural connectivity in 29% and FC in 51% of the patients studied. Our findings showed that FC frequently exists between discrete nodules and even between anatomically distant nodules, regardless of the hemisphere where the nodules were located (same or different hemispheres). These findings suggest that nodules may be connected between each other across multiple synapses, and/or connected to a third common area without being directly connected among themselves.

### Functional connectivity between heterotopic nodules reflects the synchrony of intracerebral epileptic activity between nodules

This study established the neuronal basis of the hemodynamic-based FC between heterotopic nodules. Synchrony of interictal epileptic activity between nodules, represented by the gamma envelope of the iEEG, is more likely to be detected between functionally connected nodules on fMRI. In other words, hemodynamic-based FC between heterotopic nodules reflects the synchrony of intranodular epileptic activity between these nodules, indicating that some identifiable nodules are part of an actual interictal internodular epileptic network as detected using fMRI, a noninvasive tool.

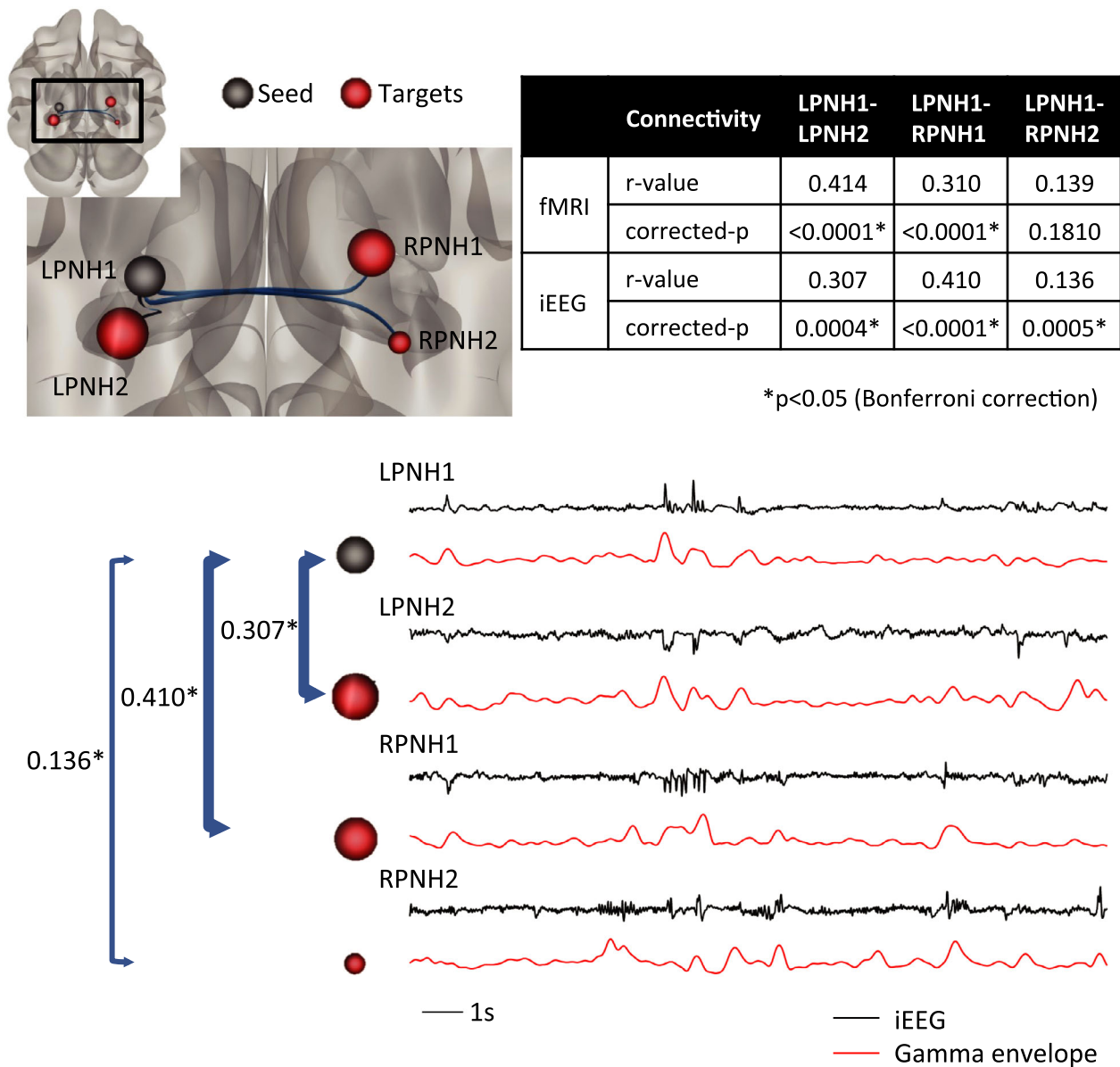


**Figure 2.** Example showing the correspondence between fMRI and intracerebral EEG in the measurement of functional connectivity between heterotopic nodules (patient 5). Top left: Internodular functional connectivity (FC) measured using functional MRI (fMRI). The seed nodule (LPNH1) is gray and the target nodules are red. The size of the spheres corresponds to the *r*-value: the larger the sphere, the higher the FC with the seed (*r*-value). The blue lines indicate the connection between LPNH1 and other nodules. Top right: FC measured using fMRI and using intracerebral EEG (iEEG). Bottom: Sample of raw iEEG traces (black line) and the corresponding gamma envelope (red line). The width of the blue double head arrows corresponds to the *r*-value measured using iEEG: the wider the arrows, the higher the FC (*r*-value). Higher synchrony was observed in nodule pairs with higher FC measured using fMRI.

### The role of functional connectivity between nodules in heterotopia-related epilepsy

What is the role of the internodular connections in heterotopia-related epilepsy? We sought to answer this question by analyzing the seizures of these patients using two different approaches. We demonstrated that ictal

activity spreads faster between connected nodules than between unconnected nodules. This finding indicates that internodular connections provide a pathway that facilitates the spread of ictal activity. On the other hand, a stronger FC between heterotopic nodules is also associated with their more frequent simultaneous involvement at seizure onset indicating that strongly connected

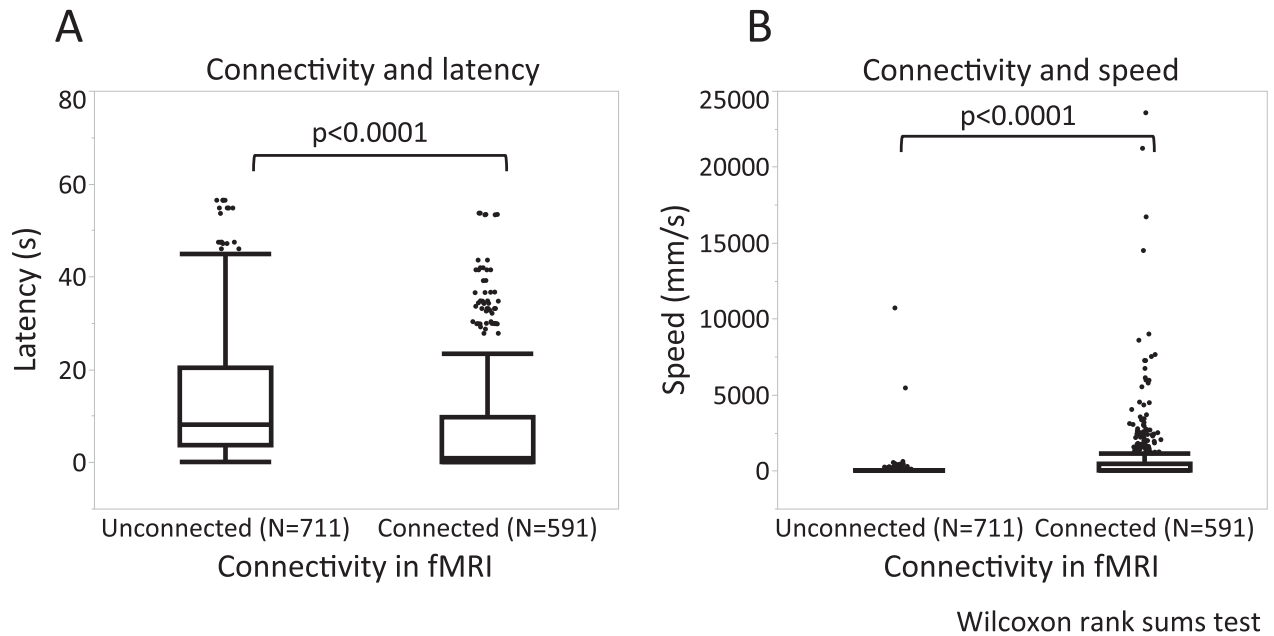


**Figure 3.** Difference in seizure spread between connected and unconnected nodules. The latency for the appearance of ictal activity was significantly shorter between channels of connected nodule pairs than that of unconnected nodule pairs, based on functional connectivity (FC) measured using functional MRI (fMRI) (A). The speed of ictal activity spread was significantly higher between channel pairs from connected nodule pairs than that of unconnected nodule pairs, based on FC in fMRI (B). Note that the speed of ictal activity spread was not available in four connected nodule pairs because ictal activity started at the same time in the two nodules in these pairs (i.e., speed =  $\infty$  when time difference = 0).

nodules may also work as a single unit in seizure generation. Cossu and colleagues showed that stereo-EEG-guided radiofrequency thermo-coagulation proved to be a safe and effective option in a small case-series of single nodular heterotopia-related focal epilepsy.<sup>18</sup> For those with multiple nodules, a surgical intervention that does not address the nodules per se or does not address all the nodules is usually less or not effective.<sup>4,6,17</sup> In this context, measuring the FC between nodular heterotopia can help identify the key interconnected nodules and select the ones to treat when there are several.

### Methodological considerations and limitations

The rate of significant connection between nodules in this study is higher than that reported in a previous study.<sup>12</sup> This is most likely because of methodological differences; we included much more fMRI data (one 6.4-min scan in the previous study versus seven to 15 6.3-min scans in this study) and performed a second-level analysis that picks up the FCs that are consistent across scans in each patient. We find this approach more robust because connectivity measures fluctuate between scans and thus one 6-min scan may not be representative of the connectivity

in each patient. Our approach also helped to avoid connectivity measures being affected by the difference of acquisition duration between patients.

Studying the neuronal activity of fMRI using iEEG recordings made separately suffers from possible temporal sampling mismatch. To limit the effect of this mismatch, we selected the iEEG recording best-matched to the fMRI by sampling the iEEG recording with a vigilance state similar to that present during the fMRI acquisition and by sampling the same duration of iEEG recording as the fMRI total acquisition time. It is interesting that, despite the different nature of the BOLD and iEEG measurements and their nonsimultaneous acquisition, we were able to establish a solid correspondence between them, thus allowing one to provide information about the other. Simultaneous iEEG and fMRI analysis may be the most direct way to study the electrophysiological basis of hemodynamic-based networks. However, it is not available in our institution and it also has a critical limitation for this type of study, the BOLD signal drop-out in the nodules, caused by intracranial electrodes placed in the lesion. Since not all nodules were sampled, the verification of fMRI-based FC between nodules in this study is limited. Also, because this is a retrospective study with limited number of patients and none of the interventions performed were

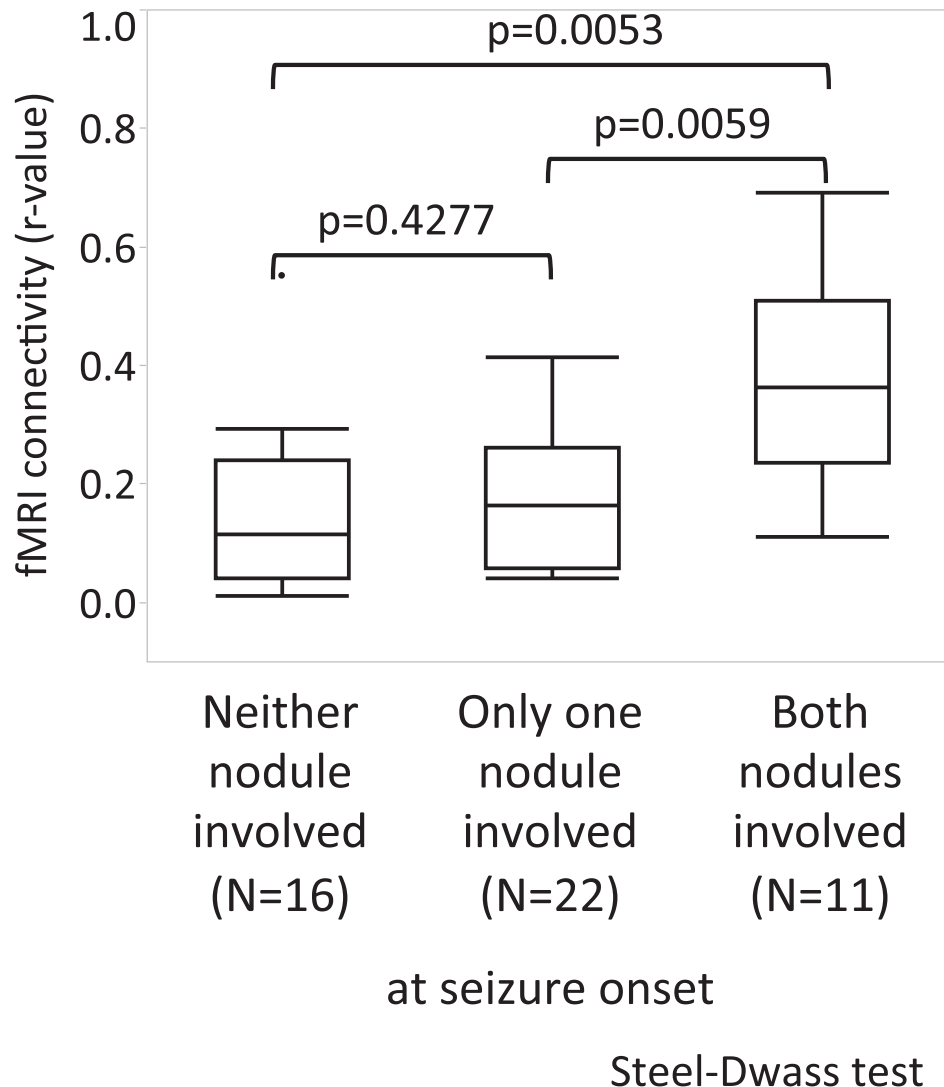


**Figure 4.** Seizure onset and functional connectivity between heterotopic nodule pairs. The *r*-value was significantly higher in nodule pairs in which both the nodules were involved at seizure onset, compared to the pairs in which one or none of the nodules was involved at seizure onset.

based on internodular FC findings, a meaningful conclusion could not be drawn from the outcome of the interventions (Table S1). The validity of fMRI-based internodular FC in clinical practice will be better defined in a larger prospective study, where most nodules are targeted with iEEG electrodes and intervention (especially thermo-coagulation) performed based in part on internodular FC findings with post-procedure iEEG recorded.

## Conclusions

Discrete heterotopic nodules are often functionally interconnected. These connections, which can be detected using fMRI, correspond to the synchrony of interictal

epileptic activity between the nodules and represent the ability of these nodules to generate synchronous seizure onsets or rapid seizure spread. Our findings may help to understand the complexity of the epileptogenic network in patients with multiple nodular heterotopia and better target the likely epileptogenic nodules.

## Acknowledgment

This work was supported by the Canadian Institutes of Health Research (FDN 143208). H.M.K. is supported by Grant-in-Aid for Scientific Research (18H06261) from the Ministry of Education, Culture, Sports, Science and Technology of Japan, and was supported by Mark Rayport

and Shirley Ferguson Rayport fellowship in epilepsy surgery and the Preston Robb fellowship of the Montreal Neurological Institute (Canada), a research fellowship of the Uehara Memorial Foundation (Japan), travel grants from Osaka Medical Research Foundation for Intractable Diseases (Japan) and Japan Epilepsy Research Foundation (Japan). F.D. is supported by a grant from Savoy Foundation (Canada).

The authors thank DK Nguyen (University of Montreal) for his help in patient recruitment, all the MRI technicians for their dedication in acquiring good quality MRI data and the EEG-lab technicians, especially Lorraine Allard and Nicole Drouin, for their dedication in iEEG acquisitions.

## Author Contributions

H.M.K., N.V.E., and J.G. were responsible for conception and design of the study. H.M.K., N.V.E., N.Z., F.D., and J.H. were responsible for acquisition and analysis of data. H.M.K., N.V.E., F.D., and J.G. were responsible for drafting a significant portion of the manuscript or figures.

## Conflict of Interest

The authors report no disclosures relevant to the manuscript.

## References

1. Watrin F, Manent JB, Cardoso C, Represa A. Causes and consequences of gray matter heterotopia. *CNS Neurosci Ther* 2015;21:112–122.
2. Dubeau F, Tampieri D, Lee N, et al. Periventricular and subcortical nodular heterotopia. A study of 33 patients. *Brain* 1995;118(Pt 5):1273–1287.
3. Valton L, Guye M, McGonigal A, et al. Functional interactions in brain networks underlying epileptic seizures in bilateral diffuse periventricular heterotopia. *Clin Neurophysiol* 2008;119:212–223.
4. Aghakhani Y, Kinay D, Gotman J, et al. The role of periventricular nodular heterotopia in epileptogenesis. *Brain* 2005;128(Pt 3):641–651.
5. Francione S, Kahane P, Tassi L, et al. Stereo-EEG of interictal and ictal electrical activity of a histologically proved heterotopic gray matter associated with partial epilepsy. *Electroencephalogr Clin Neurophysiol* 1994;90:284–290.
6. Tassi L, Colombo N, Cossu M, et al. Electroclinical, MRI and neuropathological study of 10 patients with nodular heterotopia, with surgical outcomes. *Brain* 2005;128(Pt 2):321–337.
7. Pizzo F, Roehri N, Catenio H, et al. Epileptogenic networks in nodular heterotopia: a stereoelectroencephalography study. *Epilepsia* 2017;58:2112–2123.
8. Tyvaert L, Hawco C, Kobayashi E, et al. Different structures involved during ictal and interictal epileptic activity in malformations of cortical development: an EEG-fMRI study. *Brain* 2008;131(Pt 8):2042–2060.
9. Kobayashi E, Bagshaw AP, Grova C, et al. Grey matter heterotopia: what EEG-fMRI can tell us about epileptogenicity of neuronal migration disorders. *Brain* 2006;129(Pt 2):366–374.
10. Hannan AJ, Servotte S, Katsnelson A, et al. Characterization of nodular neuronal heterotopia in children. *Brain* 1999;122(Pt 2):219–238.
11. Kakita A, Hayashi S, Moro F, et al. Bilateral periventricular nodular heterotopia due to filamin 1 gene mutation: widespread glomeruloid microvascular anomaly and dysplastic cytoarchitecture in the cerebral cortex. *Acta Neuropathol* 2002;104:649–657.
12. Christodoulou JA, Walker LM, Del Tufo SN, et al. Abnormal structural and functional brain connectivity in gray matter heterotopia. *Epilepsia* 2012;53:1024–1032.
13. Shafi MM, Vernet M, Klooster D, et al. Physiological consequences of abnormal connectivity in a developmental epilepsy. *Ann Neurol* 2015;77:487–503.
14. Kothare SV, VanLandingham K, Armon C, et al. Seizure onset from periventricular nodular heterotopias: depth-electrode study. *Neurology* 1998;51:1723–1727.
15. Liu W, Hu X, An D, et al. Disrupted intrinsic and remote functional connectivity in heterotopia-related epilepsy. *Acta Neurol Scand* 2018;137:109–116.
16. Li LM, Dubeau F, Andermann F, et al. Periventricular nodular heterotopia and intractable temporal lobe epilepsy: poor outcome after temporal lobe resection. *Ann Neurol* 1997;41:662–668.
17. Mirandola L, Mai RF, Francione S, et al. Stereo-EEG: diagnostic and therapeutic tool for periventricular nodular heterotopia epilepsies. *Epilepsia* 2017;58:1962–1971.
18. Cossu M, Fuschillo D, Cardinale F, et al. Stereo-EEG-guided radio-frequency thermocoagulations of epileptogenic grey-matter nodular heterotopy. *J Neuro Neurosurg Psychiatry* 2014;85:611–617.
19. Khoo HM, Hao Y, von Ellenrieder N, et al. The hemodynamic response to interictal epileptic discharges localizes the seizure-onset zone. *Epilepsia* 2017;58:811–823.
20. Khoo HM, von Ellenrieder N, Zazubovits N, et al. Epileptic networks in action: synchrony between distant hemodynamic responses. *Ann Neurol* 2017;82:57–66.
21. Whitfield-Gabrieli S, Nieto-Castanon A. Conn: a functional connectivity toolbox for correlated and anticorrelated brain networks. *Brain Connect* 2012;2:125–141.

22. Alakorkko T, Saarimaki H, Glerean E, et al. Effects of spatial smoothing on functional brain networks. *Eur J Neurosci* 2017;46:2471–2480.
23. Olivier A, Germano IM, Cukiert A, Peters T. Frameless stereotaxy for surgery of the epilepsies: preliminary experience. Technical note. *J Neurosurg* 1994;81:629–633.
24. Hall JA, Khoo HM. Robotic-assisted and image-guided MRI-compatible stereoelectroencephalography. *Can J Neurol Sci* 2018;45:35–43.
25. Ives JR. New chronic EEG electrode for critical/intensive care unit monitoring. *J Clin Neurophysiol* 2005;22:119–123.
26. Frauscher B, Bernasconi N, Caldairou B, et al. Interictal hippocampal spiking influences the occurrence of hippocampal sleep spindles. *Sleep* 2015;38:1927–1933.
27. Silber MH, Ancoli-Israel S, Bonnet MH, et al. The visual scoring of sleep in adults. *J Clin Sleep Med* 2007;3:121–131.
28. Mercier L, Del Maestro RF, Petrecca K, et al. New prototype neuronavigation system based on preoperative imaging and intraoperative freehand ultrasound: system description and validation. *Int J Comput Assist Radiol Surg* 2011;6:507–522.
29. Frauscher B, Dubeau F. Physiological activity and artefacts in the human epileptic brain studied with intracerebral depth electrode EEG. In: S. Lhatoo, P. Kahane, H. Lüders, eds. *Invasive studies of the human epileptic brain: principles and practice*. pp. 65–83. New York: Oxford University Press, 2018.
30. Sheen VL, Ganesh VS, Topcu M, et al. Mutations in ARFGEF2 implicate vesicle trafficking in neural progenitor proliferation and migration in the human cerebral cortex. *Nat Genet* 2004;36:69–76.
31. Fox JW, Lamperti ED, Eksioglu YZ, et al. Mutations in filamin 1 prevent migration of cerebral cortical neurons in human periventricular heterotopia. *Neuron* 1998;21:1315–1325.

### Supporting Information

Additional supporting information may be found online in the Supporting Information section at the end of the article.

**Table S1.** Interventions undertaken and the outcomes.